Seismic evidence for distinct anisotropy in the innermost inner core

FENGLIN NIU[1]* AND QI-FU CHEN[2]

[1]Department of Earth Science, Rice University, 6100 Main Street, Houston, Texas 77005, USA
[2]Institute of Earthquake Science, China Earthquake Administration, No. 63 Fuxing Avenue, Beijing, 100036, China
*e-mail: niu@rice.edu

Published online: 28 September 2008; doi:10.1038/ngeo314

Knowledge of the seismic structure of the innermost inner core is important for understanding the formation of the inner core[1–3]. It has been suggested recently that this region may exhibit distinct seismic anisotropy[4,5]. Here, we use the difference in travel times between seismic waves reflected at the underside of the inner core boundary and those traversing the inner core to constrain the seismic anisotropy. We calculated travel-time residuals for waves generated by two deep earthquakes that occurred in Indonesia and Argentina respectively, recorded by seismic arrays in Venezuela and China. The travel-time residuals are systematically larger, by about 1.8 s, for waves that travel roughly along the equatorial plane of the inner core (Indonesia–Venezuela) than for those travelling in a direction at an angle of ∼28° to the equatorial plane (from Argentina to China). The difference in travel times is arguably most sensitive to the structure near the centre of the Earth, and thus provides evidence for deep layering within the inner core. Our results are consistent with models invoking seismic anisotropy of the innermost inner core with the slowest direction tilted at an angle of ∼45° to the equatorial plane[4].

Seismic studies of the inner core using body waves, such as PKIKP, are always hindered by contamination from mantle heterogeneities. An effective way to eliminate mantle contamination is to use differential travel time or relative amplitude between PKIKP and a reference phase that travels along a very close ray path to PKIKP in the mantle. Waves reflected at or refracted above the inner-core boundary (ICB), PKiKP and PKPbc, have frequently been used to study the top ∼400 km of the inner core[6–8]. On the other hand, no appropriate reference phase has been identified for modelling the deeper part of the inner core[9]. As a result, the seismic structure of the inner ∼800 km of inner core is less constrained as compared with the outer ∼400 km.

We found that PKIIKP is an ideal reference phase to PKIKP for deciphering seismic structure at the centre of the Earth. PKIIKP traverses the inner core from either the minor-arc or the major-arc direction. Following the naming convention of surface waves, hereafter we refer to them as PKIIKP1 and PKIIKP2 for the minor- and major-arc phase, respectively. Ray paths of PKIIKPs are very close to those of PKIKP in the mantle (Fig. 1a). The maximum separation between the two phases is about 50 km in the upper mantle. In addition, both PKIIKPs and PKIKP propagate almost vertically across the D″ layer, and subsequently experience the minimum influence from seismic structure within the D″ layer (Fig. 1a).

In general, it is difficult to observe PKIIKP because of the weak reflection at the ICB (ref. 10). For deep earthquakes, however,

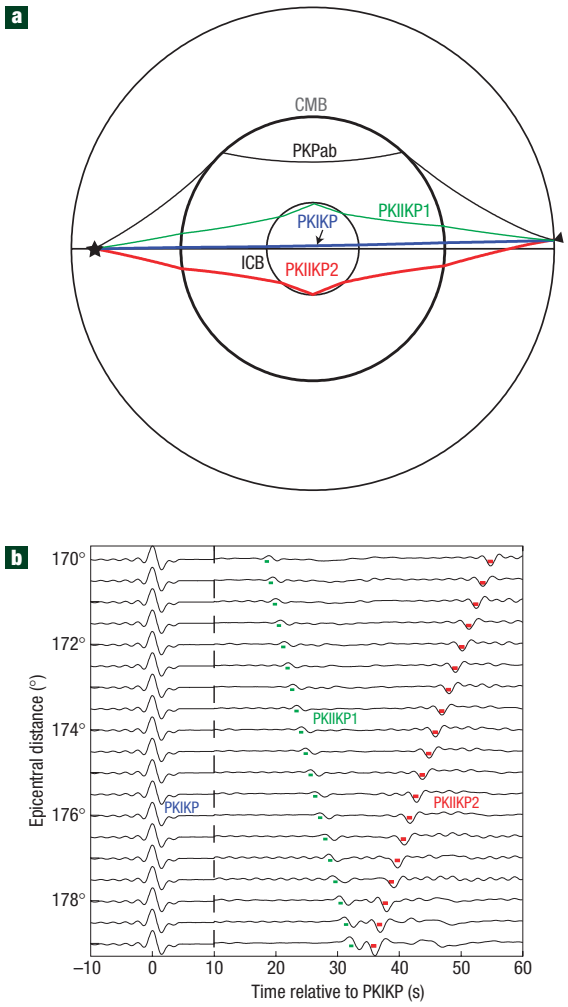

Figure 1 Ray paths and synthetic seismograms of the core phases. a, Ray paths of the core phases: PKIKP (blue), PKPab (black), PKIIKP1 (green) and PKIIKP2 (red) at an epicentral distance of 178°. ICB: inner-core boundary; CMB: core-mantle boundary. **b**, Synthetic seismograms calculated by the direct-solution method[13]. PREM and the Harvard CMT solution were used in the calculation. A single azimuth was assumed for all of the stations. Waveforms after 10 s indicated by the vertical dashed line are amplified by a factor of 10. The PREM arrival time is indicated by green and red squares for PKIIKP1 and PKIIKP2, respectively.

Table 1 Source parameters and the estimated differential travel times.

Origin time		Epicentre		Depth	Mw	Array	Distance*	PKIIKP1–PKIKP†			PKIIKP2–PKIKP†		
Date	Time	Lat. (°)	Lon. (°)	(km)			(deg)	C(s)	O(s)	O–C(s)	C(s)	O(s)	O–C(s)
06/06/2004	09:38:07.3	−6.04	113.11	579	5.9	BOLIVAR	176.05	27.3	29.2	1.9	41.7	43.5	1.8
21/03/2005	12:23:54.1	−24.98	−63.47	579	6.9	CDSN	177.94	30.4	30.3	−0.1	37.8	37.8	0

*Distance is measured from the epicentre to the centre of the array.

†C(s): calculated differential travel time in seconds based on PREM; O(s): measured differential travel time in seconds; O-C(s): differential travel-time residual.

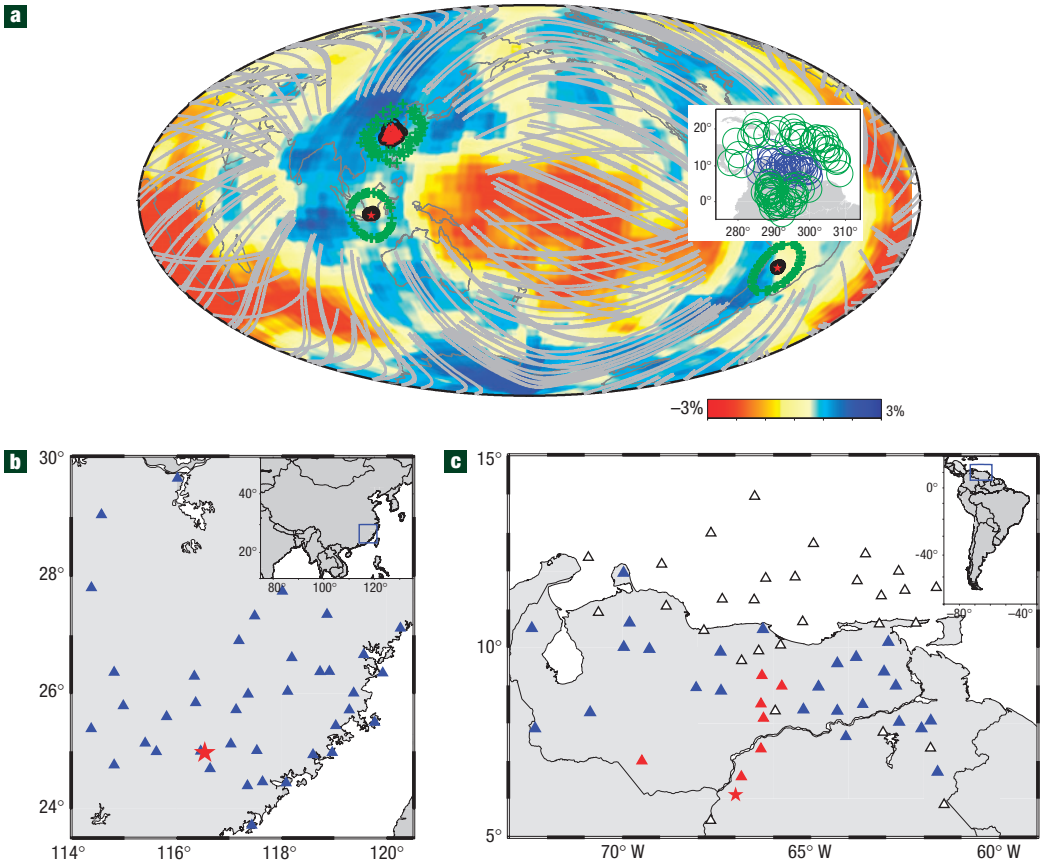

Figure 2 Map of the earthquakes and the arrays. a, Map showing inner-core ray segment of PKIIKP1/2. S-wave velocity variations of the D″ layer from Grand[30] are shown in colour. Crosses and open circles indicate the entrance and exit points at the CMB of PKIIKP1/2 and PKIKP. The inset shows the exit points of PKIKP (blue) and PKIIKP (green) of the Indonesia–Venezuela ray paths. The stars indicate the epicentres of the two earthquakes. **b**,**c**, Map of the CDSN (**b**) and BOLIVAR (**c**) stations. The insets show their geographic locations. Stars indicate the antipodes of the earthquakes. Red triangles show stations with visible PKIIKP2. Stations marked by open triangles were not used in stacking owing to a low SNR.

PKIIKP waves arrive ~18–55 s after the first arrival which lies in the quiet time window that has no primary arrivals (Fig. 1b). There are only three places on continents that are located at the opposite sides of deep earthquakes: northern Africa, northern South America and eastern central China. Seismic array data are available at the last two locations. We found clear PKIIKP arrivals from two deep-focus earthquakes that occurred in Indonesia and Argentina, respectively (Table 1, Fig. 2a). The Indonesia event was recorded by 61 stations of a PASSCAL deployment in Venezuela known as the BOLIVAR array (Fig. 2c), whereas the Argentina earthquake was recorded by 40 short-period and broadband mixed stations that belong to the China Digital Seismic Network (CDSN) (Fig. 2b). The Indonesia-BOLIVAR and the Argentina-CDSN ray paths inside the inner core are ~8° and ~28° from the equatorial plane. Thus, a comparison of the two directions can offer a decisive diagnosis of deep inner-core anisotropy.

Owing to a favourable source mechanism to antipodal stations[11], the BOLIVAR recordings of the Indonesia event show a clearly identifiable PKIIKP2 that has a reversed polarity to PKIKP (red arrows in Fig. 3a). PKIIKP1 is also visible with a polarity similar to PKIKP (green arrow in Fig. 3a) at the farthest station. These observations are consistent with Preliminary Reference Earth Model[12] (PREM) synthetic seismograms (Fig. 1b)[13]. The PKIIKP1 polarity reflects a combination of the effects of a negative reflection at the ICB (ref. 10) and a $\pi/2$ phase shift produced by the internal caustic surface for underside reflection waves[14]. Another $\pi/2$ phase

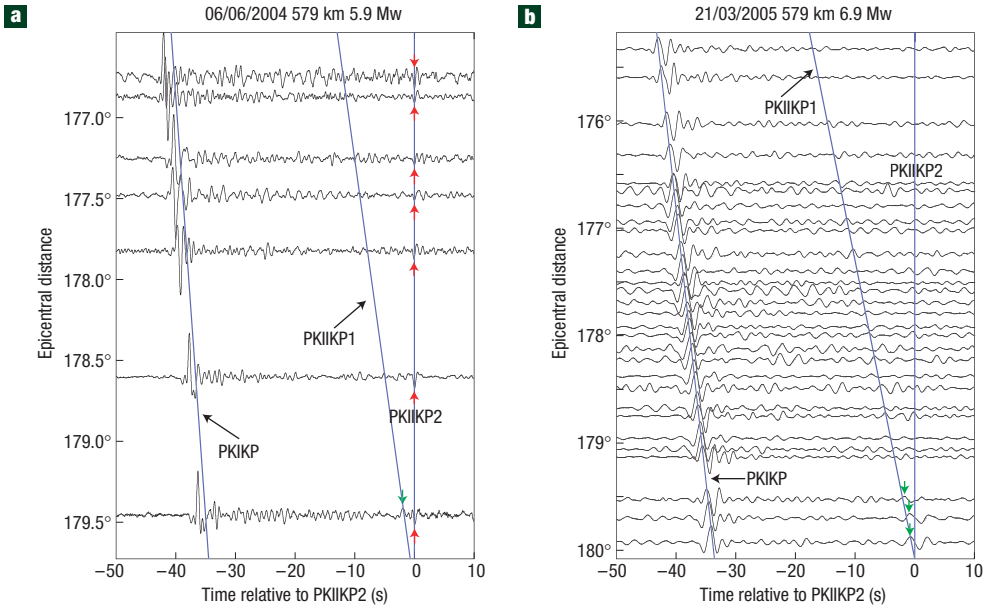

Figure 3 Examples of seismograms recorded by the two arrays. a, BOLIVAR seismograms, aligned according to the hand-picked PKIIKP2 arrival times. **b**, CDSN seismograms, aligned based on the PREM-predicted PKIIKP2 arrival times. Observed PKIIKP1 and PKIIKP2 arrivals are indicated by green and red arrows, respectively. PREM predictions of PKIKP and PKIIKP1 are shown by straight lines. All of the seismograms are filtered with the WWSSN short-period instrument response. The data are further filtered with a 2 s low-pass filter for stacking. The raw short-period BOLIVAR data are shown only for presentation purposes. The CDSN data shown here are the low-pass filtered ones.

shift is further added to the major-arc PKIIKP2 phase for crossing the antipode[15,16]. The Argentina earthquake, on the other hand, exhibits no obvious PKIIKP arrivals in the CDSN records except for the three stations near its antipode where the convergence of the PKIIKP waves from all back azimuths leads to a significant increase of their amplitude (green arrow in Fig. 3b).

To detect the PKIIKP phases and to better determine the PKIIKP–PKIKP time, we applied a second-order phase-weight slant stacking technique[17] to the data (see Methods section). Both PKIIKP phases are clearly identifiable in the vespagrams of the two events with a positive and a negative slowness relative to PKIKP. Except for PKIIKP1 of the Indonesia event, the observed slowness is in good agreement with the PREM prediction (Fig. 4a,b). The measured differential travel times of PKIIKP1–PKIKP and PKIIKP2–PKIKP and their residuals with respect to PREM are listed in Table 1. For each event, estimates of PKIIKP1–PKIKP and PKIIKP2–PKIKP residual time agree very well with each other. The Indonesia-BOLIVAR path exhibits a ~1.8 s positive travel-time residual, whereas the Argentina-CDSN path shows no anomaly with respect to PREM (Table 1, Fig. 4). Beam-forming analysis[10] (see Methods section) indicates that the two PKIIKP phases were received by the two arrays in the great-circle ray-path direction (Fig. 4c–f).

It is unlikely that the differential travel-time residuals can be explained with heterogeneities near the core–mantle boundary (CMB). In Fig. 2a, inset we plot the exit points of PKIKP and PKIIKP at the CMB of the Indonesia earthquake using different colours, with blue (PKIKP) and green (PKIIKP) circles centred at the exit points. The size of the circles is similar to the Fresnel zone of PKIKP and PKIIKP at the CMB, which is approximately 210 km for a 0.5 Hz vertically propagating P wave. The separation between the PKIIKP and PKIKP is around 400 km at the CMB, resulting in an overlap of the Fresnel zone of the two phases. Large-scale heterogeneities (a few hundreds of kilometres) near the CMB would thus affect both phases similarly and are expected to have little effect on the differential travel time.

Small-scale (a few tens of kilometres) velocity perturbations could affect the differential travel times differently, resulting in positive and negative mixed residuals among stations within the arrays, which were not observed. There is little difference in PKIIKP2–PKIKP times picked from individual seismograms (Fig. 3a). Mixed residuals could also cause destructive stacking, resulting in weak PKIIKPs that are contradictory to the large amplitudes observed in the vespagrams.

PKIKP and PKIIKP waves propagate nearly vertically across the D″ layer; the total travel times of the two phases within the lowermost 200 km of the mantle are ~28 and ~31 s, respectively. If the observed 1.8 s differential travel-time residual is accumulated solely in the D″ layer along either the PKIKP or PKIIKP ray path, then a D″ model with a 6% P-wave velocity anomaly across the entire 200 km depth is required. Otherwise, models that have a 3% anomaly across the entire D″ layer near both the entrance and exit points of PKIKP and another 3% anomaly with an opposite sign near those of the PKIIKP ray paths are needed. The entrance (or exit) regions of the two waves actually overlap with each other when their Fresnel zone size is taken into account. Thus, models requiring mixed anomalies can in principle be ruled out. Current three-dimensional P-wave velocity models[18] predict that the mantle contribution to the differential travel time is less than 0.2 s, much smaller than the observed 1.8 s. Ultralow velocity zones are observed to have a P-wave velocity reduction of ~10% with a maximum thickness of 50 km (ref. 19). The maximum travel-time anomaly they can introduce is ~0.4 s, not sufficient to explain the observed anomaly.

The PKIIKP–PKIKP differential travel time is also insensitive to Earth's ellipticity[20] (see Methods section) and changes in inner-core

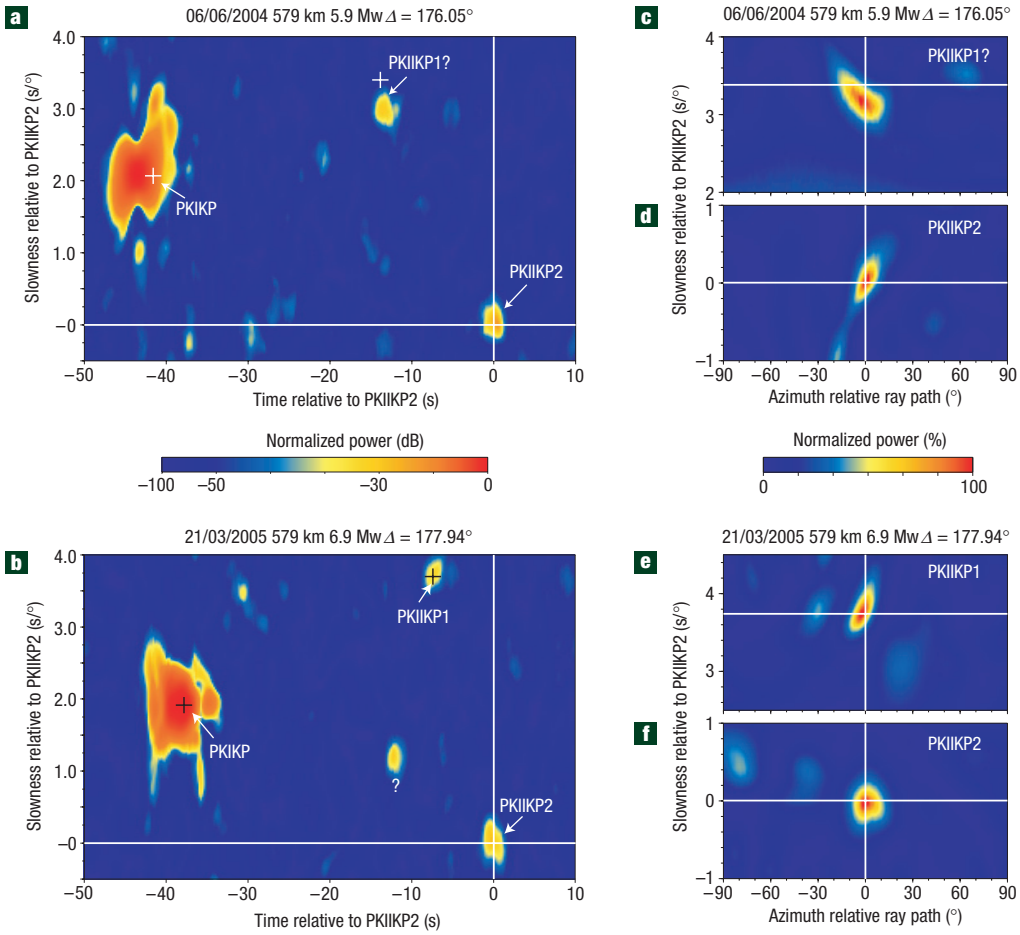

Figure 4 Results of stacking and beam-forming analyses. a,**b**, Vespagrams of the BOLIVAR (**a**) and the CDSN (**b**) data. 'Hotter' colour clusters represent greater energy. PKIKP and PKIIKP1/2 are identified by arrows with crosses denoting the theoretical arrival time and slowness calculated from the PREM model. Time and slowness are relative to PKIIKP2. Note the earlier arrival of PKIKP in **a**. The observed slowness of PKIIKP1 in **a** is slightly lower than the PREM prediction, which could be caused by ICB topography, interference with other phases and the constant slowness assumption in the slant stacking. **c**–**f**, Beam power showing the arrival slowness and back azimuth of the two PKIIKP phases.

radius (Fig. 1). Our ray tracing indicated that a 1 km increase in the inner-core radius results in only a 0.04 s change in the differential travel time, and consequently the observed large residual time is unlikely to be caused by variations in inner-core radius[21]. It is also difficult to explain the observed residual times with a possible error in source location. A 10 km error in the hypocentre depth results in a change of differential travel time by only 0.01 s, whereas a 10 km error in the epicentral location could lead to a change of differential travel time by as much as 0.17 s. Because of the wide distribution in station azimuth (Fig. 2a), a large error in the epicentral location will result in positive and negative mixed travel-time residuals among the stations within the arrays, which is not observed in the data.

Thus, the observed differential travel-time residuals can be attributed only to the heterogeneity and/or anisotropy within the inner core. Here, we further argue that the origin of the differential travel-time residuals lies in the centre of the Earth. PKIIKPs travel through only the top ~80 km of the inner core and half of their ray paths in the inner core falls roughly in the 'eastern hemisphere' and the other half in the 'western hemisphere'. The degree-one heterogeneity in the uppermost inner core thus has little effect on the travel time of PKIIKPs, which is estimated to be <0.1 s based on the E1/W1 models[22]. The inner-core ray segments of the PKIIKP phases in our data set have a global coverage of almost 70% (Fig. 2a), which makes it hard to argue for any small-scale velocity anomalies near the ICB (ref. 23) as plausible origins of the observed residuals. In fact, there is also a significant amount of crossing and overlap of PKIIKP rays between the two events; any anomalies along the PKIIKP rays will show up in the data of both events. Thus, the observed travel-time residuals are best explained by earlier PKIKP arrivals.

Both the Indonesia–Venezuela and Argentina–China paths belong to the so-called equatorial paths in which the ray angles are less than 30° from the equatorial plane, making it hard to explain the difference by existing anisotropic models with the fast direction parallel to the rotation axis[24,25]. The uppermost ~400 km of the inner core, which is well constrained from differential travel-time studies, is also expected to produce no significant travel-time anomalies to PKIKP according to current inner-core models[26]. Thus, the observed differential travel-time residuals must originate from the deeper portion of the inner core. Within this deeper region, PKIKP rays of the two paths are separated by <280 km, smaller than the Fresnel zone of the 0.5 Hz PKIKP wave. Consequently, any localized heterogeneity centred along one PKIKP ray path will affect the other path as well. Thus, the

observed 1.8 s travel-time residual along the Indonesia–Venezuela PKIKP ray path can be explained only by seismic anisotropy with the slowest propagation direction being tilted away from the equator.

Our data have no resolution on the depth distribution of the distinct anisotropy and nature of the transition between the two anisotropic regimes. Our observation here is consistent with the innermost inner core (IMIC) model[4] derived from catalogue PKIKP travel-time data. The IMIC has a radius of 300 km with the slowest direction ~45° from the equatorial plane. Transition between the IMIC and the rest of the inner core is observed to be gradual[27]. Thus, the tilted anisotropy could be distributed smoothly over a wide range of depth in the innermost ~800 km of the inner core. Both hexagonal close-packed and body-centred-cubic crystal aggregates are found to be able to produce anisotropy that matches seismic observations[28,29]. Thus, the two anisotropic regimes may be caused by different crystal structure or different proportions of the hexagonal close-packed and body-centred cubic crystals at different depths. It could also reflect a change of fabric alignment with depth, suggesting that different episodes may have existed in the growth history of the inner core.

METHODS

PHASE-WEIGHT SLANT STACKING

Let $s_{n,m}$ represent the amplitude at the mth station at the nth time for the case with M stations. For a given slowness of p, the phase-weighted stack[17] $a_n(p)$ is given by

$$a_n(p) = \frac{1}{M}\sum_{m=1}^{M} s_{n+\tau_m,m}\left|\frac{1}{M}\sum_{m=1}^{M}\exp\{i\varphi_{n+\tau_m,m}\}\right|^N,$$

where $\varphi_{n,m}$ is the instantaneous phase calculated from $s_{n,m}$ and its Hilbert transform $H[s_{n,m}]$:

$$\varphi_{n,m} = a\tan\{H[s_{n,m}]/s_{n,m}\}.$$

τ_m is the time lag of the mth station and is related to slowness p by $\tau_m = D_m \cdot p$, where D_m is the epicentral distance for the mth station minus the epicentral distance of the centre of the array. N is the power index of the phase-weight stacking and we used $N = 2$. We pre-processed the broadband data first with a deconvolution of instrument response, and then a convolution with the WorldWide Standardized Seismograph Network (WWSSN) short-period instrument response. The WWSSN short-period data seemed to possess the best signal-to-noise ratio (SNR) for the PKIKP and PKIIKP phases. We further filtered the data with a 2 s low-pass filter. A SNR > 2 was used to select the data for the final processing. We then manually picked the first peak of the PKIKP waves and aligned them at the picked times. The slowness assumed for each stack is varied with respect to that of the PKIKP arrivals (defined as zero) in increments of 0.1 s deg^{-1} within the range of ±3 s deg^{-1}. The resulting 61 stacked waveforms are subsequently converted to amplitude envelopes using the Hilbert transform. The maximum amplitude is chosen from all 61 stacked traces and is used to normalize the traces in units of decibels.

BEAM-FORMING ANALYSIS

The slant stacking analysis described above assumes that the later phases arrive from the same back azimuth as that of PKIKP. To check this assumption, we used another array analysis technique, the so-called beam-forming method. In a beam-forming analysis, all of the seismograms are linearly stacked after a time correction calculated from the assumed slowness and back azimuth. The best slowness and back azimuth were determined when the summed amplitude reaches a maximum. More specifically, we first aligned the seismograms so that PKIKP arrivals coincide with the PREM arrival time. We varied the slowness from 0 to 3 s deg^{-1} for PKIIKP1 and −3 to 0 s deg^{-1} for PKIIKP2 in increments of 0.1 s deg^{-1}. The azimuth was deviated from the great circle within the range of ±90 at increments of 1°. A 2 s time window centred on the peak PKIIKP arrival times was used to calculate the beam power.

ELLIPTICITY CORRECTION

We used the method of Kennett & Gudmundsson[20] to calculate the ellipticity corrections. PKIIKP was not included in the phase list of Kennett & Gudmundsson[20], and was computed by a combination of two PKIKP legs with the subtraction of a PKiKP segment:

$$T^{\mathrm{PKIIKP}}(z_s, \Delta) = T^{\mathrm{PKIKP}}(z_s, \Delta_a) + T^{\mathrm{PKIKP}}(0, \Delta_b) - T^{\mathrm{PKiKP}}(0, \Delta_c),$$

where z_s is the source depth and Δ_a, Δ_b and Δ_c are the arc lengths of the two PKIKP legs and the PKiKP leg, respectively. They were calculated by matching the ray parameter of the PKIIKP phase.

Received 11 November 2007; accepted 27 August 2008; published 28 September 2008.

References

1. Jacobs, J. A. The Earth's Inner Core. *Nature* **172**, 297–298 (1953).
2. Buffett, B. A. in *Earth's Deep Interior: Mineral Physics and Seismic Tomography From the Atomic to Global Scale* Vol. 117 (eds Karato, S. *et al.*) 37–62 (Geophys. Monogr. Ser., AGU, Washington, 2000).
3. Yoshida, S., Sumita, I. & Kumazawa, M. Growth model of the inner core coupled with the outer core dynamics and the resulting elastic anisotropy. *J. Geophys. Res.* **101**, 28085–28104 (1996).
4. Ishii, M. & Dziewonski, A. M. The innermost inner core of the earth: Evidence for a change in anisotropic behaviour at the radius of about 300 km. *Proc. Natl Acad. Sci.* **99**, 14026–14030 (2002).
5. Beghein, C. & Trampert, J. Robust normal mode constraints on inner-core anisotropy from model space search. *Science* **299**, 552–555 (2003).
6. Niu, F. & Wen, L. Hemispherical variations in seismic velocity at the top of the Earth's inner-core. *Nature* **410**, 1081–1084 (2001).
7. Creager, K. C. Anisotropy of the inner core from differential travel times of the phases PKP and PKIKP. *Nature* **356**, 309–314 (1992).
8. Tanaka, S. & Hamaguchi, H. Degree one heterogeneity and hemispherical variation of anisotropy in the inner core from PKP(BC)–PKP(DF) times. *J. Geophys. Res.* **102**, 2925–2938 (1997).
9. Breger, L., Tkalcic, H. & Romanowicz, B. The effects of D on PKP (AB-DF) travel time residuals and implications for inner core structure. *Earth Planet. Sci. Lett.* **175**, 133–143 (2000).
10. Aki, K. & Richards, P. G. *Quantitative Seismology* (W. H. Freeman, New York, 1980).
11. Dziewonski, A. M., Chou, T.-A. & Woodhouse, J. H. Determination of earthquake source parameters from waveform data for studies of global and regional seismicity. *J. Geophys. Res.* **86**, 2825–2852 (1981).
12. Dziewonski, A. M. & Anderson, D. L. Preliminary reference Earth model. *Phys. Earth Planet. Inter.* **25**, 297–356 (1981).
13. Takeuchi, N., Geller, R. J. & Cummins, P. R. Highly accurate P-SV complete synthetic seismograms using modified DSM operators. *Geophys. Res. Lett.* **23**, 1175–1178 (1993).
14. Choy, G. L. & Richards, P. G. Pulse distortion and Hilbert transformation in multiply reflected and refracted body waves. *Bull. Seismol. Soc. Am.* **65**, 55–70 (1975).
15. Brune, J. N., Nafe, J. E. & Alsop, L. E. The polar phase shift of surface waves on a sphere. *Bull. Seismol. Soc. Am* **51**, 247–257 (1961).
16. Rial, J. & Cormier, V. Seismic waves at the epicentre's antipode. *J. Geophys. Res.* **85**, 2661–2668 (1980).
17. Schimmel, M. & Paulssen, H. Noise reduction and detection of weak, coherent signals through phase-weighted stacks. *Geophys. J. Int.* **130**, 497–505 (1997).
18. Fukao, Y., Widiyantoro, S. & Obayashi, M. Stagnant slabs in the upper and lower mantle transition zone. *Geophys. Rev.* **39**, 291–323 (2001).
19. Garnero, E. J. & Thorne, M. in *Earth's ULVZ: Ultra-Low Velocity Zone, in Encyclopedia of Geomagnetism and Paleomagnetism* (eds Gubbins, D. & Herrero-Bervera, E.) (Springer, Netherlands, 2008).
20. Kennett, B. L. N. & Gudmundsson, O. Ellipticity corrections for seismic phases. *Geophys. J. Int.* **127**, 40–48 (1996).
21. Souriau, A. & Souriau, M. Ellipticity and density at the inner core boundary from subcritical PKiKP and PcP data. *Geophys. J. Int.* **98**, 39–54 (1989).
22. Wen, L. & Niu, F. Seismic velocity and attenuation structures in the top of the Earth's inner core. *J. Geophys. Res.* **107**, doi:10.1029/2001JB000170 (2002).
23. Vidale, J. E. & Earle, P. S. Fine-scale heterogeneity in the Earth's inner core. *Nature* **404**, 273–275 (2000).
24. Morelli, A., Dziewonski, A. M. & Woodhouse, J. H. Anisotropy of the inner core inferred from PKIKP travel times. *Geophys. Res. Lett.* **13**, 1545–1548 (1986).
25. Shearer, P. M., Toy, K. M. & Orcutt, J. A. Axi-symmetric Earth models and inner-core anisotropy. *Nature* **333**, 228–232 (1988).
26. Creager, K. C. in *Earth's Deep Interior: Mineral Physics and Seismic Tomography From the Atomic to Global Scale* Vol. 117 (eds Karato, S. *et al.*) 89–114 (Geophys. Monogr. Ser., AGU, Washington, 2000).
27. Cormier, V. F. & Stroujkova, A. Waveform search for the innermost inner core. *Earth Planet. Sci. Lett.* **236**, 96–105 (2005).
28. Steinle-Neumann, G., Stixrude, L., Cohen, R. E. & Gulseren, O. Elasticity of iron at the temperature of the Earth's inner core. *Nature* **413**, 57–60 (2001).
29. Belonoshko, A., Skorodumova, V., Rosengren, A. & Johansson, B. Elastic anisotropy of Earth's inner core. *Science* **319**, 797–800 (2008).
30. Grand, S. P. Mantle shear-wave tomography and the fate of subducted slabs. *Phil. Trans. R. Soc. A* **360**, 2475–2491 (2002).

Acknowledgements

We thank the BOLIVAR team, FUNVISIS (Venezuelan Foundation for Seismological Research) and CEA (China Earthquake Administration) for providing the data, N. Takeuchi for providing the SMD code and H. Kawakatsu and S. Tanaka for helpful discussions. This work is supported by Rice University and the NSF.

Author information

Reprints and permission information is available online at http://npg.nature.com/reprintsandpermissions. Correspondence and requests for materials should be addressed to F.N.